A. Mertol[1]
Assoc. Mem. ASME

R. Greif
Mem. ASME

Department of Mechanical Engineering,
University of California,
Berkeley, Calif. 94720

Y. Zvirin
Faculty of Mechanical Engineering,
Technion,
Israel Institute of Technology,
Haifa, Israel

Two-Dimensional Study of Heat Transfer and Fluid Flow in a Natural Convection Loop

A study has been made of the heat transfer and fluid flow in a natural convection loop. Previous studies of these systems have utilized a one-dimensional approach which requires a priori specifications of the friction and the heat-transfer coefficients. The present work carries out a two-dimensional analysis for the first time. The results yield the friction and the heat-transfer coefficients and give their variation along the loop with the Graetz number as a parameter. Comparison is also made with experimental data for the heat flux and good agreement is obtained.

Introduction

A study has been made of the heat transfer and fluid flow in a laminar natural convection loop which is created by heating from below and cooling from above. The driving force for a natural convection loop results from the density difference between the lower and the upper portions of the loop. Previous studies of such loops have utilized a one-dimensional approach by averaging the governing equations over the cross section (see Creveling et al. [1, 2], Damerell and Schoenhals [3], Greif, Zvirin, and Mertol [4], and Bau and Torrance [5]). Studies on a number of natural convection loops have been carried out by Keller [6], Welander [7], Japikse [8], Zvirin et al. [9–11], Torrance et al. [12, 13], Huang [14], Gillette et al. [15], and Mertol et al. [16, 17]. Natural convection loops, in general, have many applications including the production of geothermal energy, solar heating, and the emergency cooling of nuclear reactors. Although most applications involve turbulent flows, many laminar natural convection flows do appear, particularly in solar systems.

The present work differs from the previous studies of natural convection loops in that a two-dimensional analysis is carried out for the first time. It is noted that the previous studies which followed a one-dimensional approach required a priori specifications of the friction and the heat-transfer coefficients, f and h, respectively. One result of the present study is that the Graetz number, Gz, now emerges as a parameter, and it is shown that the quantity fRe varies as a nonmonotonic function of Gz. Another common assumption has been the use of a constant heat-transfer coefficient, h. The present results show the variation of h with respect to distance along the thermosyphon with Gz as a parameter. Results have also been obtained for the detailed temperature and velocity profiles, as well as for averages of these quantities. Lastly, comparison with the experimental data of Creveling et al. [1, 2] shows good agreement.

Analysis

The analysis which follows is for the determination of the velocity and temperature profiles in a toroidal thermosyphon. The loop is heated continuously by a constant heat flux, q, over the bottom half and is cooled continuously over the top half by transferring heat to the surface which is maintained at the constant temperature, T_w. (see Fig 1). Variations in both the radial, r, and axial, θ, directions are considered. Axial symmetry is assumed and axial conduction, viscous dissipation, and the effects of curvature have been neglected. Fluid properties are assumed to be constant except for the evaluation of the density in the buoyancy term of the momentum equation. The flow is assumed to be laminar and to be in the axial, θ, direction; i.e., radial and azimuthal velocities are neglected. With these assumptions, we obtain from the equation of continuity for incompressible flow that the velocity in the θ-direction is only a function of the radius:

$$v = v(r) \tag{1}$$

The momentum equation in the θ-direction is given by

$$0 = -\frac{1}{R}\frac{dp}{d\theta} - \rho g \cos\theta + \frac{\mu}{r}\frac{d}{dr}\left(r\frac{dv}{dr}\right) \tag{2}$$

Integrating equation (2) along the loop and using the relation $\rho = \rho_w[1 - \beta(T - T_w)]$ in the buoyancy term yields

$$0 = \frac{\rho_w g \beta}{2\pi}\int_0^{2\pi}(T - T_w)\cos\theta \, d\theta + \mu\left(\frac{d^2v}{dr^2} + \frac{1}{r}\frac{dv}{dr}\right) \tag{3}$$

Note that the pressure term has been eliminated by the integration around the loop. Consequently, the use of the momentum equation in the r-direction is not required. The energy equation is given by the following relation:

$$\frac{v}{R}\frac{\partial T}{\partial \theta} = \alpha\left(\frac{\partial^2 T}{\partial r^2} + \frac{1}{r}\frac{\partial T}{\partial r}\right) \tag{4}$$

Note that axial conduction is neglected.

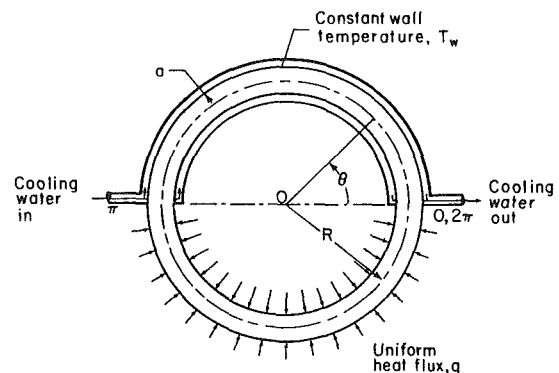Equations (3) and (4) must be solved simultaneously subject to the following boundary conditions:

Fig. 1 The circular, toroidal natural circulation loop

$$\frac{dv}{dr}\bigg|_{r=0} = 0 = \frac{\partial T}{\partial r}\bigg|_{r=0} \qquad (5a)$$

$$v(a) = 0 \qquad (5b)$$

$$T(a,\theta) = T_w \quad \text{for} \quad 0 < \theta < \pi \qquad (5c)$$

$$k\frac{\partial T}{\partial r}\bigg|_{r=a} = q \quad \text{for} \quad \pi < \theta < 2\pi \qquad (5d)$$

Equations (3–5) are made dimensionless according to the following definitions:

$$\phi = \frac{T-T_w}{qa/k}, \quad w = \frac{v}{V}, \quad \xi = \frac{r}{a} \quad \text{and} \quad \eta = \xi Gz^{1/2} \qquad (6)$$

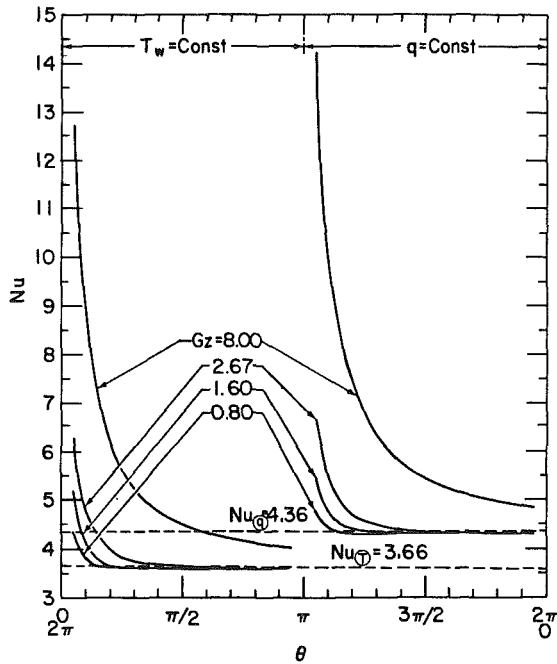where V is the characteristic velocity defined by Creveling et al. [1]

Fig. 2 Nusselt number variation along the loop for different Graetz numbers

$$V = \left(\frac{g\beta Raq}{2\pi c\mu}\right)^{1/2} \qquad (7)$$

The Graetz number, Gz, and the characteristic Reynolds number are defined by

$$Gz = Re_{ch}Pr\left(\frac{2a}{2\pi R}\right) = \frac{2\rho_w ca^2 V}{\pi kR}, \quad Re_{ch} = \frac{\rho_w V2a}{\mu} \qquad (8)$$

The dimensionless form of equations (3–5) then becomes:

$$0 = \int_0^{2\pi} \phi\cos\theta d\theta + \frac{2}{\pi}\left(\frac{d^2w}{d\eta^2} + \frac{1}{\eta}\frac{dw}{d\eta}\right) \qquad (9)$$

$$w\frac{\partial\phi}{\partial\theta} = \frac{2}{\pi}\left(\frac{\partial^2\phi}{\partial\eta^2} + \frac{1}{\eta}\frac{\partial\phi}{\partial\eta}\right) \qquad (10)$$

$$\frac{dw}{d\eta}\bigg|_{\eta=0} = 0 = \frac{\partial\phi}{\partial\eta}\bigg|_{\eta=0} \qquad (11a)$$
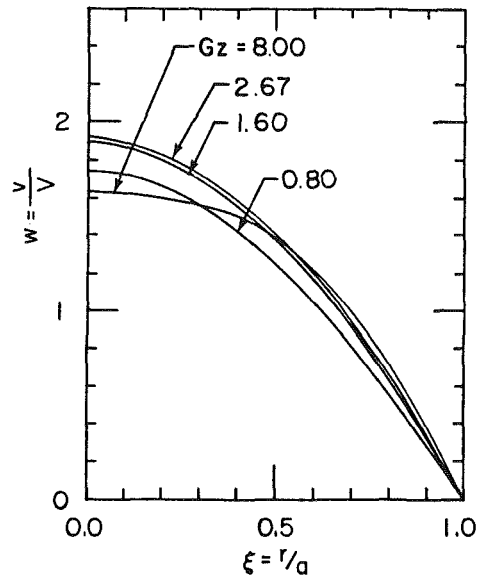
$$w(Gz^{1/2}) = 0 \qquad (11b)$$

Fig. 3 Velocity distribution

Nomenclature

a = radius of the toroid, Fig. 1

c = specific heat

f = friction coefficient, equations (12) and (13)

G = mass flow rate

Gz = Graetz number, equation (8)

g = acceleration of gravity

h = heat-transfer coefficient, equation (15)

k = thermal conductivity

Nu = Nusselt number, equation (15)

Pr = Prandtl number, $\frac{\mu c}{k}$

p = pressure

q = heat flux

R = radius of the circular loop (see Fig. 1)

Re = Reynolds number, equation (14)

Re_{ch} = characteristic Reynolds number, equation (8)

r = radial space coordinate, $r = 0$ is center of tube

T = temperature

V = characteristic velocity, equation (7)

v = velocity

$\bar{v}$ = cross-sectional average velocity

w = dimensionless velocity, equation (6)

$\bar{w}$ = dimensionless cross-sectional average velocity

Greek Symbols

α = thermal diffusivity, $\frac{k}{\rho_w c}$

β = thermal expansion coefficient

η = dimensionless modified radial space coordinate, equation (6)

θ = axial space coordinate

μ = absolute viscosity

ξ = dimensionless radial space coordinate, equation (6)

ρ = density

ϕ = dimensionless temperature, equation (6)

ϕ_b = dimensionless bulk temperature, equation (16)

ϕ_w = dimensionless wall temperature for the lower loop

Subscripts

0 = location at $\theta = 0$

1 = location at $r = 0$ ($\xi = 0$)

b = bulk

ch = characteristic

i = axial space step in the finite difference equations

j = radial space step in the finite difference equations

M = location at $\theta = 2\pi$

N = location at $r = a$ ($\xi = 1$)

w = wall

$$\phi(Gz^{1/2},\theta) = 0 \quad \text{for} \quad 0 < \theta < \pi \tag{11c}$$

$$\frac{\partial \phi}{\partial \eta}\bigg|_{\eta = Gz^{1/2}} = Gz^{-1/2} \quad \text{for} \quad \pi < \theta < 2\pi \tag{11d}$$

In terms of presenting results the friction factor and the Nusselt number are also calculated. The friction factor, f, is defined by

$$f = -\frac{\mu \dfrac{dv}{dr}\bigg|_{r=a}}{\frac{1}{2}\rho_w \bar{v}^2} \tag{12}$$

where $\bar{v}$ is the average velocity over the cross section given by

$$\bar{v} = \int_0^a v(r) \, 2\pi r \, dr / \pi a^2.$$

On a dimensionless basis, f becomes

$$f = -\frac{4}{Re} \frac{Gz^{1/2}}{\bar{w}} \frac{dw}{d\eta}\bigg|_{\eta = Gz^{1/2}} \tag{13}$$

where $\bar{w}$ is the average dimensionless velocity over the cross section,

$$\bar{w} = \bar{v}/V = \frac{2}{Gz} \int_0^{Gz^{1/2}} w\eta d\eta,$$

and Re is the Reynolds number defined by

$$Re = \frac{\rho_w \bar{v} 2a}{\mu} = \frac{Gz \, \bar{w}}{Pr}\left(\frac{2\pi R}{2a}\right) \tag{14}$$

The Nusselt number is defined by

$$Nu(\theta) = \frac{h(\theta)2a}{k} = \begin{cases} -\dfrac{2Gz^{1/2}}{\phi_b}\dfrac{\partial \phi}{\partial \eta}\bigg|_{\eta=Gz^{1/2}} & \text{for } 0 < \theta < \pi \\ & \qquad\qquad (15a) \\ \dfrac{2}{\phi_w - \phi_b} & \text{for } \pi < \theta < 2\pi \qquad (15b) \end{cases}$$

where the bulk temperature, ϕ_b, is defined by

$$\phi_b = \frac{2}{\bar{w}Gz}\int_0^{Gz^{1/2}} \phi(\eta,\theta)w(\eta)\eta d\eta \tag{16}$$

Method of Solution

The governing equations, equations (9) and (10), have been solved numerically by using a finite difference method to calculate the temperature and the velocity distributions. The inte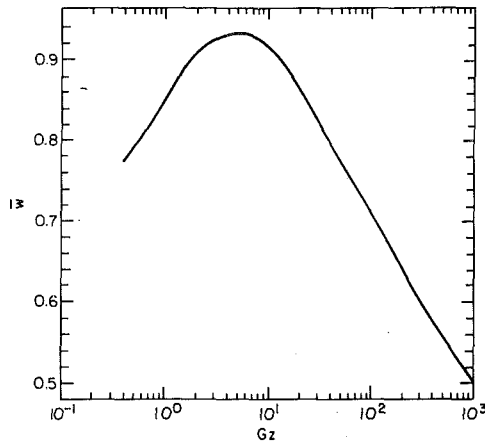gral in equation (9) was evaluated by using the trapezoidal rule and the derivatives were evaluated by using the backward difference formula. The governing equations are

$$w_j = \left\{ w_{j+1} + w_{j-1}\left(1 - \frac{1}{j}\right) \right.$$
$$+ \frac{\pi}{2}\left[\frac{1}{2}\phi_{0,j}\cos(0) + \sum_{i=1}^{M-1}\phi_{i,j}\cos(i\Delta\theta)\right.$$
$$\left.\left. + \frac{1}{2}\phi_{M,j}\cos(M\Delta\theta)\right]\Delta\theta(\Delta\eta)^2\right\} / \left(2 - \frac{1}{j}\right) \tag{17}$$

and

$$\phi_{i,j} = \left\{ w_j \phi_{i-1,j} + \frac{2}{\pi}\frac{\Delta\theta}{(\Delta\eta)^2}\left[\phi_{i,j+1}\right.\right.$$
$$\left.\left. + \phi_{i,j-1}\left(1 - \frac{1}{j}\right)\right]\right\} / \left[w_j + \frac{2}{\pi}\frac{\Delta\theta}{(\Delta\eta)^2}\left(2 - \frac{1}{j}\right)\right] \tag{18}$$
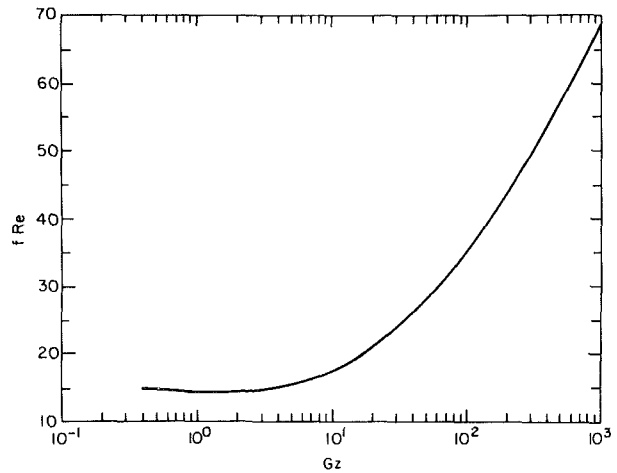
The following boundary conditions have been used:

Fig. 5 Friction coefficient as a function of the Graetz number

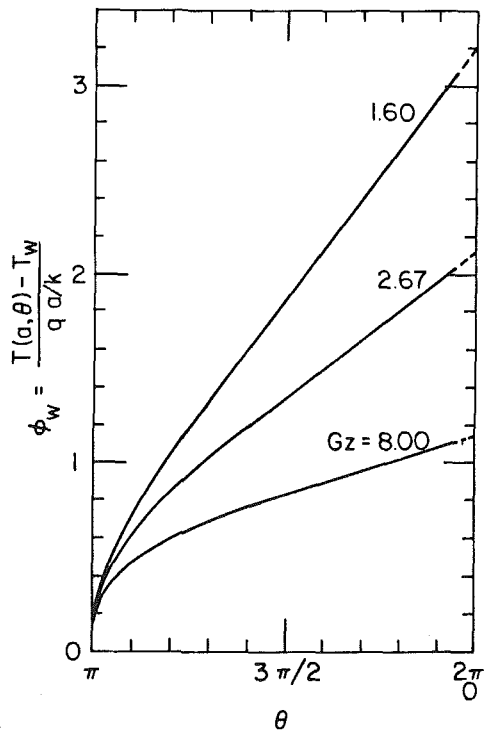Fig. 4 Average velocity as a function of the Graetz number

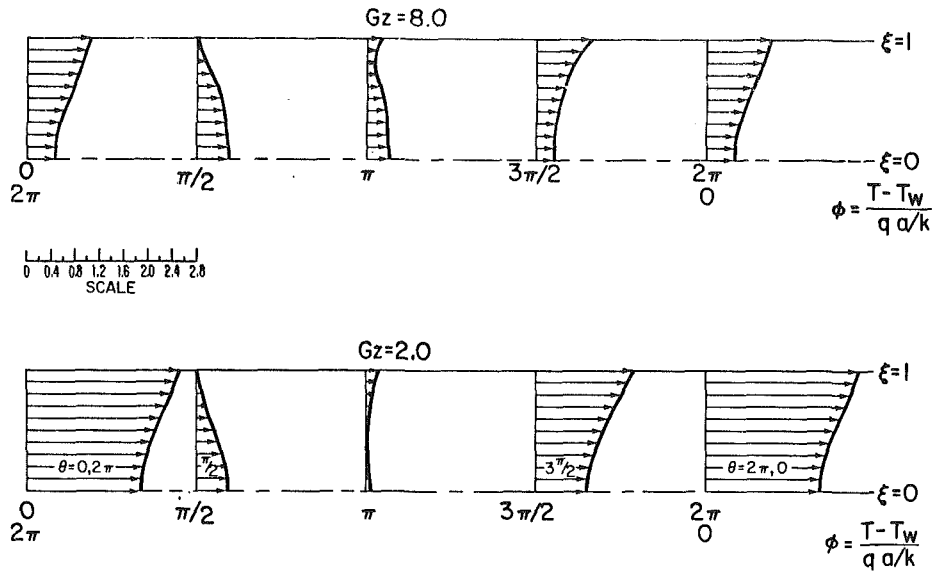Fig. 6 Wall temperature variation along the heated region of the loop

Fig. 7 Temperature distributions inside the loop

(*i*) Symmetry conditions at the centerline, $\eta = 0$ ($\xi = 0$), for the velocity:

$$w_0 = w_1 + \frac{\pi}{8}\left\{\frac{1}{2}\phi_{0,0}\cos(0) + \sum_{i=1}^{M-1}\phi_{i,0}\cos(i\Delta\theta)\right.$$

$$\left. + \frac{1}{2}\phi_{M,0}\cos(M\Delta\theta)\right\}\Delta\theta(\Delta\eta)^2 \tag{19}$$

and for the temperature:

$$\phi_{i,0} = \left[w_0\,\phi_{i-1,0} + \frac{8}{\pi}\frac{\Delta\theta}{(\Delta\eta)^2}\phi_{i,1}\right]\Big/\left[w_0 + \frac{8}{\pi}\frac{\Delta\theta}{(\Delta\eta)^2}\right] \tag{20}$$

(*ii*) Boundary conditions on the surface, $\eta = Gz^{1/2}$ ($\xi = 1$) (except at the locations $\theta = 0$, 2π and $\theta = \pi$) for the velocity:

$$w_N = 0 \text{ (no slip condition)} \tag{21}$$

and for the temperature:

$$\phi_{i,N} = 0 \quad \text{for} \quad 0 < \theta < \pi \tag{22a}$$

Using an energy balance for the heated region yields (neglecting axial convection),

$$\phi_{i,N} = \phi_{i,N-1} + \Delta\eta\,Gz^{-1/2} \quad \text{for} \quad \pi < \theta < 2\pi \tag{22b}$$

Energy balances on the surface ($\xi = 1$) are made at the locations $\theta = 0$, 2π and $\theta = \pi$. The resulting relations are given by (neglecting axial convection because of the vanishing velocity):

$$\phi_{M,N} = \phi_{M,N-1} + \frac{\Delta\eta Gz^{-1/2}}{(2 - \Delta\eta Gz^{-1/2})} \quad \text{at} \quad \theta = 0, 2\pi \tag{23a}$$

and

$$\phi_{M/2,N} = \phi_{M/2,N} - 1 + \frac{\Delta\eta Gz^{-1/2}}{(2 - \Delta\eta Gz^{-1/2})} \quad \text{at} \quad \theta = \pi \tag{23b}$$

where $\theta = i\Delta\theta$, $\eta = j\Delta\eta$, $2\pi = M\Delta\theta$ and $Gz^{1/2} = N\Delta\eta$

Equations (17–23) were solved by initially assuming parabolic velocity and temperature distributions and iterating until convergence was obtained. A space increment of $\Delta\theta$ equal to $\pi/40$ was used for all the calculations. Different values of the space increments in the radial direction, $\Delta\xi$, were used. For the larger values of the Graetz number, $\Delta\xi \sim 0.025$ and for the smaller values of the Graetz number, $\Delta\xi \sim 0.05$. Calculations were made to check the sensitivity to the space increments and showed variations for the velocity and
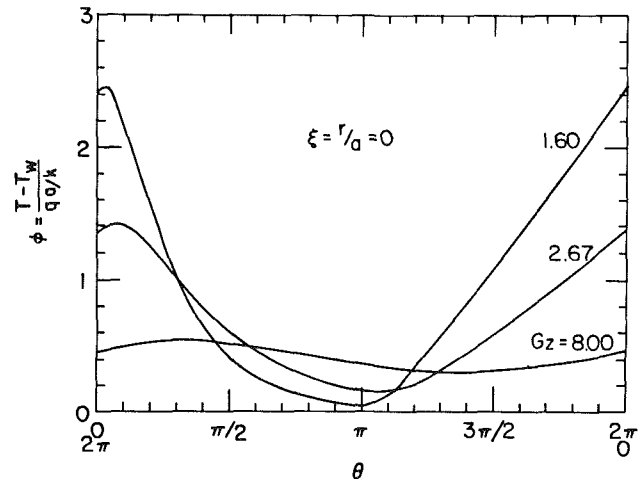

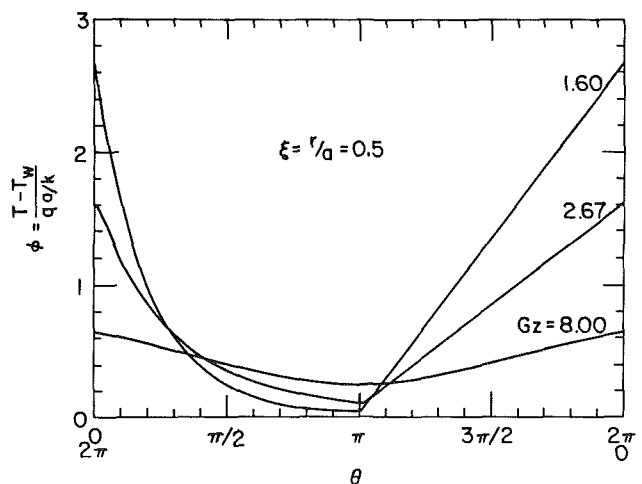Fig. 8a Centerline ($r = 0$) temperature variation along the loop

Fig. 8b Temperature variation at $r = a/2$ along the loop

temperature distributions of less than 5 percent. With respect to the calculations, it is also noted that for the cylindrical control volume adjacent to the wall, axial convection was neglected. This leads to an energy balance in the heating region that is correct to first order, cf. equations (22b), (23a), and (23b). It is also noted that the backward difference

formulation for the axial convection term generates a numerical diffusion. However, a Taylor series expansion shows that this false diffusion is of the order of $(\Delta\theta)^2$ which is smaller than the principal terms (see equation (18)). This is in accord with the sensitivity statement given above concerning the space increments.

Results and Discussion

The steady-state behavior of a natural circulation loop which is heated uniformly over the lower half and cooled by maintaining a constant wall temperature over the upper half has been investigated (see Fig. 1). A two-dimensional, axially symmetric model was used with the independent variables, ξ (or η), for the radial coordinate, and, θ, for the axial coordinate, and the parameter, Gz (defined in equation (8)) which is equal to the Graetz number. The characteristic velocity, V, results from buoyancy so that it is also possible to relate the Graetz number to a Grashof number, Prandtl number, and a diameter to length ratio. However, it is more convenient to use the Graetz number in this study.

Note that axial conduction has been neglected. This is a good approximation for large values of the Peclet number, Pe, where Pe = Gz $(2\pi R/2a)$. For slug flow, the effects of axial conduction should be considered for $0 \le$ Pe ≤ 100 [18]. For the experimental loops of references [1–3], $a = 0.015$ m and $R = 0.38$ m; this would correspond to the range $0 \le$ Gz ≤ 1.25. (This range may be altered for the present velocity profiles which result from buoyancy.) It would therefore appear that the effects of axial conduction are of importance for the lower values of the Graetz number; i.e., Gz = 0.4 and 0.8. It is noted that the range of values of the Graetz number for the experimental data [1, 2] is 44 < Gz < 172 (cf. Fig. 10) which should be consistent with the omission of axial conduction.

The increase in the heat transfer for increasing values of the Graetz number is clearly shown in Fig. 2 in both the heating region ($\pi < \theta < 2\pi$, q_w = const = q) and the cooling region ($0 < \theta < \pi$, T_w = const). For small and moderate Graetz numbers, the local Nusselt number approaches the values 4.36 and 3.66 for the heating and cooling regions, respectively. Note that these values are the asymptotic values for fully developed laminar flow inside a circular straight tube for

uniform heating and for constant wall temperature, respectively.

The behavior of the velocity profile, $w(\xi)$, and the average cross-sectional velocity, $\bar{w}$, is shown in Figs. 3 and 4 for various values of Gz. As can be seen from the figures, the average velocity (or the flow rate) increases initially with the Graetz number, due to the increase of the buoyancy driving force (as explained above by the relation between the Graetz and Grashof numbers) and the decrease in friction (cf. Fig. 5). As Gz is further increased the resistant friction force increases, as can be seen from the increase in the velocity gradient at the wall in Fig. 3 (cf. Fig. 5). The increase in friction for increasing values of the Graetz number coupled with the accompanying effect of smaller temperature differences, causes the flow rate to increase at a slower rate so that the average velocity, $\bar{w}$, reaches a maximum and then decreases (cf. Fig. 4). For completeness, it is noted that for forced laminar flow, fRe = 16.

At this point we wish to refer to the experiments of Damerell and Schoenhals [3] and their visual observations in the cooled region (close to the connection between the heated and cooled sections, i.e., at $\theta \approx 0^+$). They concluded that at this location the axial velocity, v, near the surface of the tube, was in a direction opposite to that of the main flow. The theoretical velocity profiles shown in Fig. 3 differ from these observations and this is felt to be a consequence of neglecting the radial and azimuthal components of the velocity as specified in obtaining equation (1). It is possible that this effect is most pronounced at the location noted and is of less significance in the rest of the loop. Accordingly, the inversion of the velocity profile has not been treated in this study. Further discussion of the velocity is given later in connection with the comparison of the theoretical results with the experimental data of Creveling et al. [1, 2].

Figure 6 shows the increase of the wall temperature in the heated region with increasing θ, i.e., as the fluid moves through and is heated in this region. The increase becomes smaller as the Graetz number, which characterizes the relative buoyancy effect, increases. As noted above, the heat transfer increases with Gz which results in smaller temperature differences (also see Fig. 7). This figure shows the change in the temperature distribution around the loop.

Table 1 Average velocity, bulk temperature, and friction coefficient for different Graetz numbers

| Gz	$\bar{w}$	$\theta=0,2\pi$	$\theta=\pi/2$	$\theta=\pi$	$\theta=3\pi/2$	$\phi_b(0)-\phi_b(\pi)$	fRe
			$\phi_b(\theta)$				
0.4	0.775	12.186	0.001	0.157	6.215	12.029	15.00
0.8	0.831	5.725	0.047	0.074	2.932	5.651	14.64
1.6	0.893	2.688	0.224	0.060	1.390	2.628	14.39
2.0	0.908	2.145	0.280	0.078	1.124	1.021	14.41
2.7	0.922	1.638	0.331	0.111	0.884	1.527	14.54
3.2	0.928	1.399	0.349	0.136	0.775	1.263	14.71
4.0	0.933	1.169	0.358	0.163	0.672	1.006	15.02
8.0	0.923	0.702	0.332	0.226	0.470	0.476	16.75
10.0	0.915	0.607	0.311	0.223	0.420	0.384	17.56
15.0	0.890	0.473	0.273	0.210	0.345	0.263	19.35
20.0	0.867	0.400	0.247	0.197	0.301	0.099	20.85
50.0	0.772	0.246	0.175	0.152	0.200	0.094	26.74
100.0	0.714	0.174	0.135	0.122	0.148	0.052	35.01
150.0	0.672	0.144	0.117	0.107	0.126	0.037	39.79
200.0	0.642	0.126	0.105	0.097	0.112	0.029	43.54
500.0	0.557	0.087	0.077	0.074	0.081	0.013	57.28
1000.0	0.503	0.069	0.064	0.062	0.066	0.007	68.11
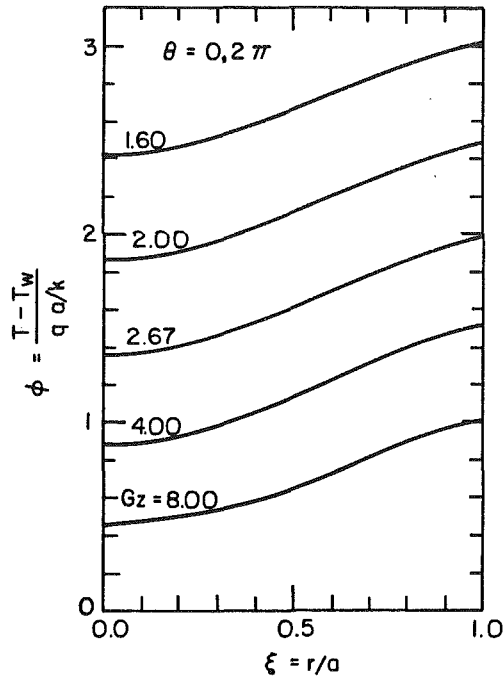
Fig. 9a   Temperature variation in the radial direction at $\theta = 0, 2\pi$

Fig. 9b   Temperature variation in the radial direction at $\theta = \pi/2$
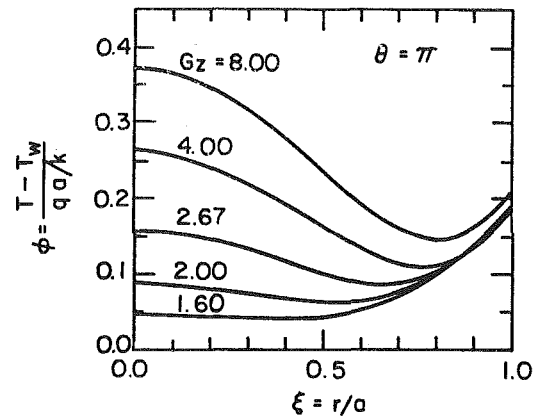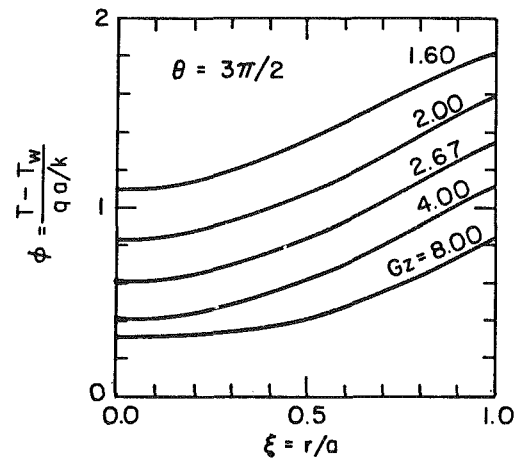

Fig. 9c   Temperature variation in the radial direction at $\theta = \pi$

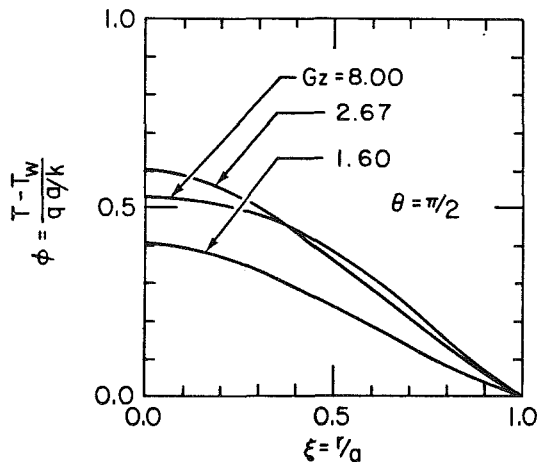Fig. 9d   Temperature variation in the radial direction at $\theta = 3\pi/2$

Fig. 10   Comparison between the theoretical and experimental values

The temperature variation with respect to θ on the axis ($r = 0$), at the mid-distance to the wall ($r = a/2$) and the bulk temperature, are shown in Figs. 8(a), 8(b) and Table 1. As can be seen for short axial distances, the centerline temperature continues to increase in the cooling section, due to radial conduction from the hotter fluid. This effect is reversed as the cooling from the wall penetrates into the fluid and the centerline temperature then decreases. The maximum temperature becomes higher and is reached sooner (for smaller values of θ) as the Graetz number decreases. This is due to the effect of increasing velocities with greater buoyancy effects, as noted above. For completeness, detailed radial temperature variations are presented in Figs. (9a–9d) for various locations around the loop.

The numerical results of the present work are compared to the experimental results of Creveling et al. [1, 2] in Fig. 10, where the mass flux $G = \rho V \bar{w}$ is plotted versus the heat flux input, q. The comparison is made in the laminar regime only. Average properties of the fluid (water) were taken at the average loop temperature as reported in [2]. The agreement between the numerical results and the data is very good. It is noted that at the higher values of q in Fig. 10, the flows are
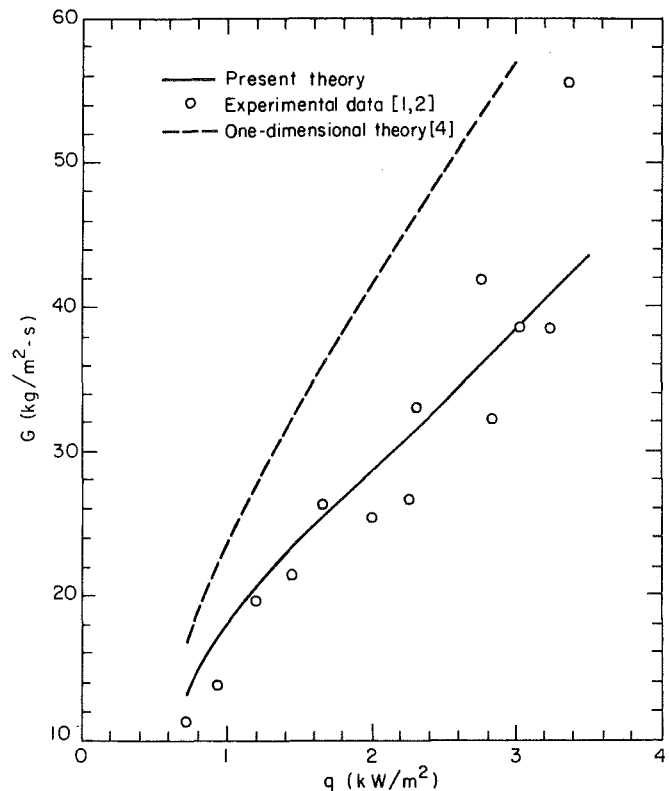
unstable, with growing oscillations and reversed flow. It was, therefore, difficult to accurately determine the flow rates and fluid temperatures in this range. For completeness, results based on one dimensional theory are also presented in Fig. 10. The fully developed flow relations, $f = 16/Re$ and $h = 1.83 \, k/a$, were used in obtaining this result [4]. Creveling et al. [1, 2] used different relations, but the disagreement between the one-dimensional theory and the data was still large.

In Fig. 10 it is seen that the mass flux $G = \rho V \bar{w}$ increases with respect to the heat input, q. The experimental range of values of the Graetz number [1, 2] is $44 < Gz < 172$, and it is noted that over this range the calculated values of $\bar{w}$ decrease for increasing Gz (cf. Fig. 4). The calculated increase of the mass flux, $G = \rho V \bar{w}$, with respect to the heat input, q, results from the stronger increase in V with respect to q, i.e., $V \sim q^{1/2}$.

Conclusions

The steady-state velocity and temperature distributions in a natural circulation toroidal loop have been obtained by a numerical solution of the coupled two-dimensional continuity, momentum, and energy equations. A single parameter, the Graetz number, Gz, (related to the Grashof number) governs the motion in the loop. The solutions were used to obtain the friction and the heat transfer. It was found that the friction parameter, fRe, varies significantly as a function of the Graetz number. The local Nusselt numbers in the heated and cooled sections decrease with axial distance, θ. For small and moderate Graetz numbers, Nu approaches the forced convection values 4.36 and 3.66 for constant heat flux and constant wall temperatures, respectively. The heat transfer increases for increasing values of the Graetz number and this is accompanied by smaller temperature differences. The present numerical predictions have been compared with the existing data for the steady state flux and good agreement has been obtained.

Acknowledgment

References

1 Creveling, H. F., De Paz, J. F., Baladi, J. Y., and Schoenhals, R. J., "Stability Characteristics of a Single-Phase Free Convection Loop," *Journal of Fluid Mechanics*, Vol. 67, 1975, pp. 65–84.

2 Creveling, H. F., "Steady Flow and Stability Characteristics of Free Convection Flow in Circulation Loops," Ph.D. dissertation, Purdue University, 1964.

3 Damerell, P. S., and Schoenhals, R. J., "Flow in a Toroidal Thermosyphon with Angular Displacement of Heated and Cooled Section," ASME JOURNAL OF HEAT TRANSFER, Vol. 101, 1979, pp. 672–676.

4 Greif, R., Zvirin, Y., and Mertol, A., "The Transient and Stability Behavior of a Natural Convection Loop," ASME JOURNAL OF HEAT TRANFER, Vol. 101, 1979, pp. 684–688.

5 Bau, H. H., and Torrance, K. E., "Transient and Steady Behavior of an Open, Symmetrically-Heated, Free Convection Loop," *International Journal of Heat and Mass Transfer*, Vol. 24, 1981, pp. 597–609.

6 Keller, J. B., "Periodic Oscillations in a Model of Thermal Convection," *Journal of Fluid Mechanics*, Vol. 26, 1966, pp. 599–606.

7 Welander, P., "On the Oscillatory Instability of a Differentially Heated Fluid Loop," *Journal of Fluid Mechanics*, Vol. 29, 1967, pp. 17–30.

8 Japikse, D., "Advances in Thermosyphon Technology," in *Advances in Heat Transfer*, edited by T. F. Irvine, Jr. and J. P. Hartnett, Vol. 9, Academic Press, New York, 1973, pp. 1–111.

9 Zvirin, Y., Shitzer, A., and Grossman, G., "The Natural Circulation Solar Heater Models with Linear and Nonlinear Temperature Distributions," *International Journal of Heat and Mass Transfer*, Vol. 20, 1977, pp. 997–999.

10 Zvirin, Y., "A Review of Natural Circulation Loops in Pressurized Water Reactors and Other Systems," EPRI Report NP-1676-SR, Jan. 1981, to appear in *Nuclear Eng. & Design*, Vol. 67, 1981, pp. 203–225.

11 Zvirin, Y., Jeuck, P. R., Sullivan, C. W., and Duffey, R. B., "Experimental and Analytical Investigation of a Natural Circulation System with Parallel Loops," ASME JOURNAL OF HEAT TRANSFER, Vol. 103, 1981, pp. 645–652.

12 Torrance, K. E., "Open-Loop Thermosyphons with Geological Applications," ASME JOURNAL OF HEAT TRANSFER, Vol. 101, 1979, pp. 677–683.

13 Bau, H. H., and Torrance, K. E., "On the Stability and Flow Reversal of an Asymmetrically Heated Open Convection Loop," *Journal of Fluid Mechanics*, Vol. 106, 1981, pp. 417–433.

14 Huang, B. J., "Similarity Theory of Solar Water Heater with Natural Circulation," *Solar Energy*, Vol. 25, 1980, pp. 105–116.

15 Gillette, J. L., Singer, R. M., Tokar, J. V., and Sullivan, J. E., "Experimental Study of the Transition from Forced to Natural Circulation in EBR-II at Low Power and Flow," ASME JOURNAL OF HEAT TRANSFER, Vol. 102, 1980, pp. 525–530.

16 Mertol, A., Greif, R., and Zvirin, Y., "The Transient, Steady State and Stability Behavior of a Thermosyphon with Throughflow," *International Journal of Heat and Mass Transfer*, Vol. 24, 1981, pp. 621–633.

17 Mertol, A., Place, W., Webster, T., and Greif, R., "Detailed Loop Model (DLM) Analysis of Liquid Solar Thermosiphons with Heat Exchangers," *Solar Energy*, Vol. 27, 1981, pp. 367–386.

18 Schneider, P. J., "Effect of Axial Fluid Conduction on Heat Transfer in the Entrance Regions of Parallel Plates and Tubes," ASME JOURNAL OF HEAT TRANSFER, Vol. 79, 1957, pp. 765–773.